

# The Compressed Baryonic Matter experiment

Sélim SEDDIKI<sup>1</sup>, on behalf of the CBM Collaboration

<sup>1</sup> *Gesellschaft für Schwerionenforschung mbH (GSI)  
Planckstraße 1, 64291 Darmstadt, Germany*

**Abstract.** The Compressed Baryonic Matter (CBM) experiment is a next-generation fixed-target detector which will operate at the future Facility for Antiproton and Ion Research (FAIR) in Darmstadt. The goal of this experiment is to explore the QCD phase diagram in the region of high net baryon densities using high-energy nucleus-nucleus collisions. Its research program includes the study of the equation-of-state of nuclear matter at high baryon densities, the search for the deconfinement and chiral phase transitions and the search for the QCD critical point. The CBM detector is designed to measure both bulk observables with a large acceptance and rare diagnostic probes such as charm particles, multi-strange hyperons, and low mass vector mesons in their di-leptonic decay. The physics program of CBM will be summarized, followed by an overview of the detector concept, a selection of the expected physics performance, and the status of preparation of the experiment.

## 1 Introduction

The CBM experiment is a fixed-target heavy-ion detector which will operate at the future FAIR facility (GSI, Darmstadt). This experiment seeks to study fundamental properties of the strong interaction and its underlying theory, the Quantum Chromo-Dynamics (QCD). Some of the most important features of the strong interaction are not quantitatively understood, like the phenomenon of color confinement in ordinary nuclear matter and the origin of most of the mass of light hadrons (thus, of most of the visible universe). In practice, CBM will study the properties of QCD matter at very high net baryon densities, in similar conditions as the ones presumably existing in the core of neutron stars.

Above a certain critical energy density, nuclear matter is believed to exist in a deconfined state of quarks and gluons. This is illustrated in Figure 1: such a state can be produced by heating and/or compressing nuclear matter. In accelerator laboratories, this is done by colliding heavy nuclei, thus creating a dense and hot fireball in the overlap region between the two nuclei. At the RHIC and the LHC colliders, collisions at ultra-relativistic energies lead to an extremely hot but almost net-baryon free fireball. According to lattice QCD, the phase transition from confined to deconfined matter at high temperatures and vanishing net baryon densities is a smooth cross-over, while at moderate temperatures but higher baryon densities a first-order phase transition may take place [1, 2]. Exploring the latter region of the QCD phase diagram, poorly known theoretically and experimentally, is the object of several physics programs at lower beam energies, which are currently carried out at SPS/CERN and RHIC/BNL and which will be continued later at NICA/JINR and FAIR. First indications of the onset of deconfinement may have already been observed by NA49 (at the SPS), and confirmed recently by

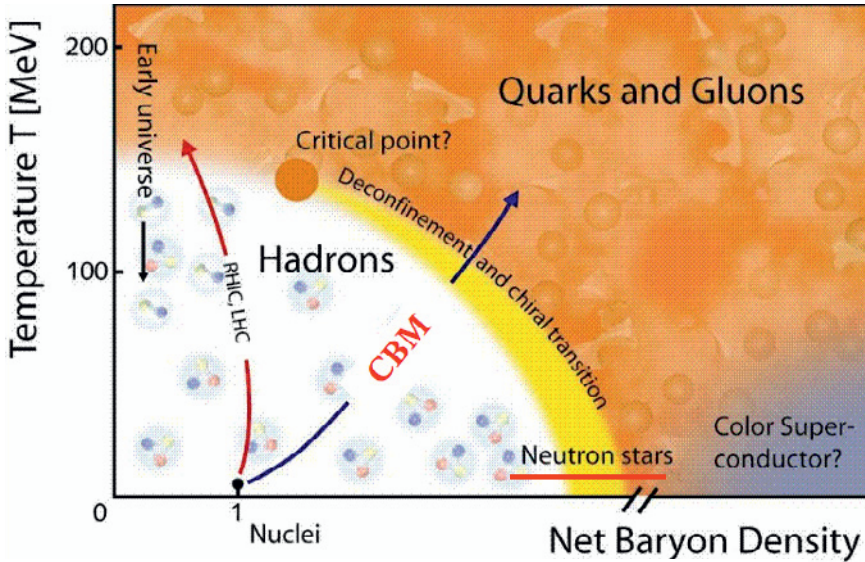


**Figure 1.** Sketch of the QCD phase diagram of nuclear matter as a function of temperature and net baryon density (see text).

STAR (at the RHIC), at a beam energy of around 30 GeV/nucleon [3, 4], which lies within the FAIR energy range.

The two different natures of the deconfinement phase transition in the high temperature and high density regions of the phase diagram suggest the existence of a QCD critical point (see Figure 1). The existence and location of this point are till today under debate since lattice QCD calculations have large systematic uncertainties at finite net baryon density [1, 2]. Figure 2 summarizes the results obtained from different lattice QCD calculations (green symbols) along with the predictions of other theoretical QCD-based models (black symbols). According to lattice QCD predictions, the critical point, if it exists, should lie in a wide region of temperatures ( $T$ ) and baryon chemical potentials ( $\mu_B$ ):  $150 \text{ MeV} < T < 200 \text{ MeV}$  and  $200 \text{ MeV} < \mu_B < 800 \text{ MeV}$ . CBM will contribute to the search for this critical point over a broad region of the QCD phase diagram.

The question of the hadron masses is supposedly related to the phenomenon of spontaneous breaking of chiral symmetry, a fundamental property of QCD (in the limit of vanishing quark masses). There are robust theoretical predictions that chiral symmetry is at least partially restored in dense matter [5], and that, among other effects, the masses of hadrons (containing light quarks) in dense baryonic matter can differ from their corresponding free masses. The study of such in-medium effects is another important goal of the CBM experiment.

An experimental evidence of the first-order phase transition, the QCD critical point and in-medium modifications of hadron masses in dense baryonic matter would be a breakthrough for understanding the properties of the strong interaction.

## 2 CBM physics program and observables

The FAIR facility will offer unique opportunities for the investigation of the QCD phase diagram at extreme net baryon densities, besides serving a variety of other research fields (hadron physics

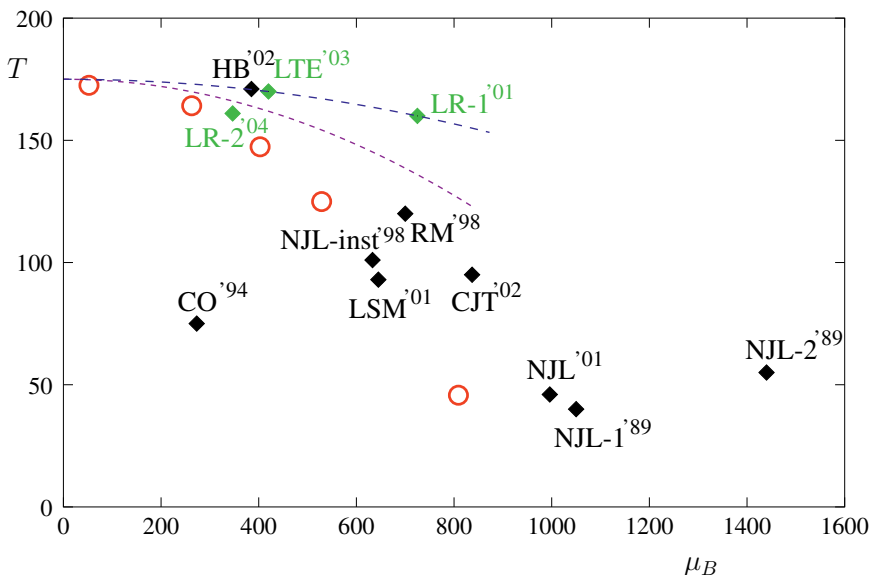


**Figure 2.** Theoretical predictions for the location of the QCD critical point in the temperature ( $T$ ) versus baryon chemical potential ( $\mu_B$ ) plane (Units are in MeV) [6]. The green symbols are the results of QCD lattice simulations while the black symbols correspond to the predictions of different QCD-based models (see [7] for details). Labels are abbreviations of models/methods used and the publication date. Uncertainties are not shown. The red circles indicate the freeze-out points obtained at various collision energies.

with anti-proton beams, nuclear structure physics with radioactive beams, and plasma physics with highly pulsed ion beams). For the nuclear collision program, two synchrotrons SIS100 and SIS300 (providing a magnetic rigidity of 100 and 300 Tm, respectively) will deliver fully stripped heavy ion beams up to uranium with extremely high intensities (of up to  $2 \times 10^9$  ions per second) at beam energies ranging from 2 to 35 GeV/nucleon. Lighter ions ( $Z/A = 0.5$ ) will be accelerated up to 45 GeV/nucleon, while proton beams will be available up to 90 GeV.

The broad energy range provided by FAIR will allow producing nuclear matter at the maximal net baryon density achievable with heavy ion collisions [8]. As shown in Figure 3, according to various transport models, the density reaches up to about twelve times the normal nuclear matter density in the core and at the early stage of central Au+Au collisions at a beam energy of 20 GeV/nucleon ( $\sqrt{s_{NN}} \sim 6.4$  GeV). As can be seen in Figure 4, this important feature of the FAIR accelerator is supported by the derived chemical freeze-out parameters that are required to reproduce, within a canonical or grand canonical statistical model, the measured particle yields in central A+A collisions at SIS, AGS, SPS and RHIC energies ( $\sqrt{s_{NN}} \sim 2, 5, 20, 200$  GeV, respectively) [9]. As the beam energy decreases a clear shift towards lower temperatures and higher  $\mu_B$  occurs.

Another important feature of this accelerator facility is that it will serve several (up to 5) experiments in parallel, allowing CBM operating with heavy ion beams up to 4 months per year. Both the unprecedented beam intensities and the high beam availability will allow CBM measuring rare probes, like charm hadrons and light vector mesons (in their di-leptonic decay), for the first time in the FAIR energy range. Note that  $\Lambda_c^+$  open charm baryons are valuable probes in heavy ion collisions at FAIR energies [11], where their relative production with respect to that of other charm hadrons is

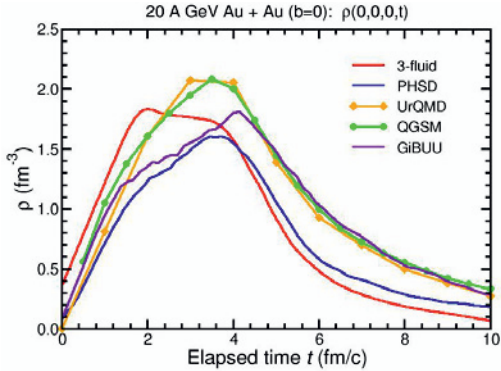


**Figure 3.** Time evolution of the net baryon density  $\rho$  at the center of a head-on Au+Au collision at a bombarding energy of 20 GeV/nucleon, as obtained with various dynamical models [8, 10].

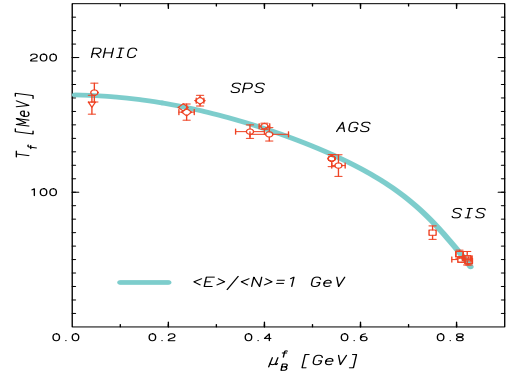


**Figure 4.** Experimental values of the chemical freeze-out points derived from a statistical model analysis of data ranging from SIS to RHIC energies [9]. The curve corresponds to a fixed energy per hadron of 1 GeV in the hadronic gas model.

expected to be important at very high net baryon density. Note also that rare probes at these energies also include multi-strange particles which are up to now scarcely measured in heavy ion collisions.

CBM is designed to perform high statistics measurements of hadronic, leptonic and photonic probes with a large acceptance. Its physics program includes a large set of observables [10], among which:

- The yield and collective flow of strange and charm hadrons, which are expected to reflect the onset of deconfinement.
- The collective flow of hadrons, which is particularly sensitive to the equation-of-state of nuclear matter at the early stage of the reactions.
- Particle production at threshold energies (strangeness at SIS100 and charm at SIS300), which can deliver important information about the equation-of-state of nuclear matter.
- Non-statistical event-by-event fluctuations of various quantities (particle yields and yield ratios) related to conserved quantum numbers (baryon, charge, and strangeness), which would signal a QCD critical point.
- In-medium modifications of hadron masses, in particular of open charm hadrons and light vector mesons, which would provide valuable insight into the expected restoration of chiral symmetry in dense baryonic matter.

The experimental task of CBM is to measure all these observables in A+A, p+A and p+p collisions as a function of collision energy and system size with high precision and statistics, and to search for discontinuities which would signal for example a first-order deconfinement phase transition. This physics program will be carried out by measuring nuclear collisions at extremely high interaction rates.

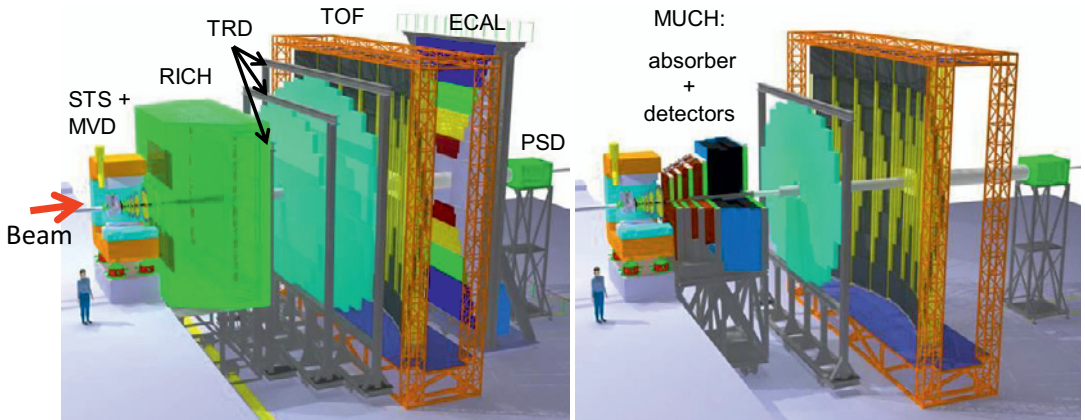


**Figure 5.** Layout of the CBM detector setup (see text). Two configurations are foreseen: one dedicated to the measurements of hadrons and electrons (left side), and another one optimized for detecting muons (right side).

### 3 CBM detector, experimental challenge and physics performance

#### 3.1 CBM detector and experimental challenge

A schematic view of the detector concept is given in Figure 5 (see [12] for details). While open charm and multi-strange hyperons will be measured through their weak decay into charged hadrons, charmonium states and light vector mesons will be detected via their decay into both di-electrons and di-muons. The CBM detector setup thus features a flexible arrangement of particle identification detectors: one configuration is dedicated to the identification of hadrons and electrons, while another one is specialized in detecting muons. The second configuration must include absorbers which can efficiently absorb all particles except muons. It is thus not compatible with the first one. In both configurations, the detector comprises a low mass Silicon Tracking System (STS) embedded inside a superconducting dipole magnet, a Transition Radiation Detector (TRD) and a Time-Of-Flight (TOF) detector. In addition, a forward hadronic calorimeter, called Projectile Spectator Detector (PSD), will serve for event characterization (collision centrality and event plane determination). The electron and hadron configuration additionally comprises a high resolution Micro-Vortex Detector (MVD), located close to the target before the STS, a Ring Imaging CHerenkov (RICH) and an Electromagnetic CALorimeter (ECAL). As for the muon configuration, these two last sub-detectors must be replaced by a MUon CHamber (MUCH), which is made of absorber layers interlaced with tracking stations. The dimensions and positions of all detectors (except the PSD) are chosen such that, for central A+A collisions at 25 GeV/nucleon and a magnetic dipole field of  $B = 1$  T, about 70% of the emitted charged particles are accepted (including mid-rapidity and forward rapidity particles, at low and high transverse momenta).

All detector components have been designed to operate at unprecedentedly high collision rates in order to perform high statistics and systematic measurements. For example, collision rates of up to 10 MHz and of the order of 100 kHz are foreseen for  $J/\psi$  and open charm measurements, respectively. This puts very strong constraints on the design of the detector components and readout electronics in terms of rate capability. Also, rare probes in A+A collisions at FAIR energies have multiplicities several order of magnitude lower than that of abundant particles (e.g. pions, protons and electrons).

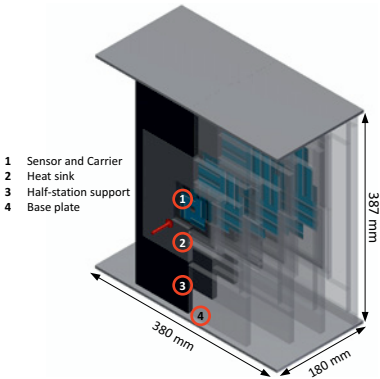


**Figure 6.** Layout of the Micro-Vortex Detector [13]. It consists of up to 4 stations, located at 5, 10, 15 and 20 cm from the target. Sensors (in blue) are arranged according to the sensor geometry expected at SIS100. Each station is divided in two half-stations, which can be moved in and out using the base plates (up and down). Are also shown the half-station support (in black) and the heat sink (in dark grey). Read-out cables, front-end electronics and the vacuum vessel are not shown for simplicity.

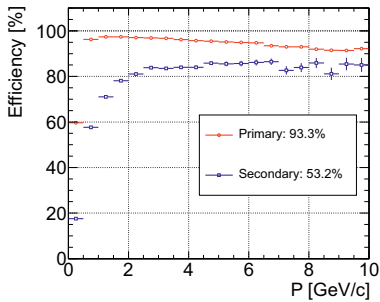


**Figure 8.** Track reconstruction efficiency for charged particles in the STS as a function of momentum in central Au(25 GeV/nucleon)+Au collisions [15]. Primary tracks are created at the collision vertex. Tracks associated with secondary particles produced in the detector are referred to as secondary tracks.

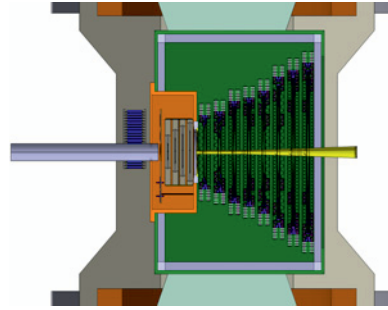


**Figure 7.** Layout of the Micro-Vortex Detector (left side), placed inside a vacuum vessel (depicted in orange), followed by the Silicon Tracking System [14]. The latter is composed of 8 stations placed from 30 cm to 1 m from the target (and separated by a step of 10 cm). All components are placed inside a temperature isolated box (depicted in green) that is inserted into the dipole magnet. This box is the supporting structure for the STS and MVD detectors, as well as for the target and the beam pipe (depicted in yellow).

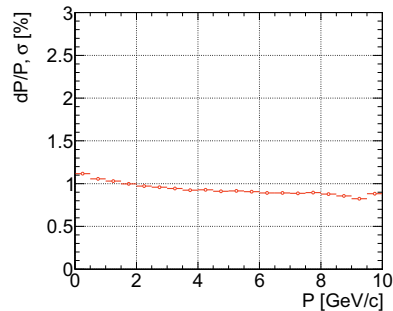


**Figure 9.** Momentum resolution for charged particles in the STS as a function of momentum in central Au(25 GeV/nucleon)+Au collisions [15].

Measuring these rare probes thus calls for very efficient background rejection strategies, which rely on the detector capability for track reconstruction and particle identification.

The STS detector will be used for the reconstruction of the trajectory of charged particles inside a magnetic dipole field and for the determination of their momentum. It consists of 8 stations of thin and high resolution double-sided silicon strip sensors, stabilized by a low mass carbon support structure [14]. The detector layout can be seen in Figure 7. Figures 8 and 9 show results of detailed detector simulation studies, including in particular a realistic material budget. These studies demonstrate a

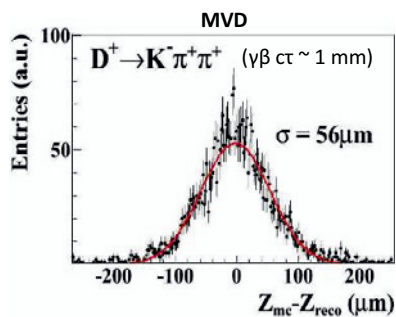


**Figure 10.** Decay vertex resolution (along the beam axis) for the  $D^+ \rightarrow \pi^+ \pi^+ K^-$  signal in central Au(25 GeV/nucleon)+Au collisions. The average decay length of  $D^+$  mesons at this beam energy is  $\sim 1$  mm in the laboratory frame.

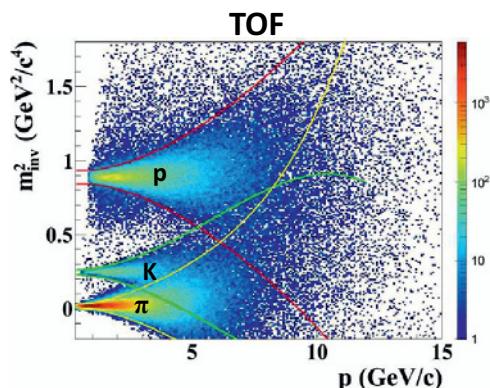


**Figure 11.** Squared mass reconstructed for pions, kaons and protons as a function of momentum, using the combined STS and TOF detectors [16].

high track reconstruction efficiency (of about 95%) and a good momentum resolution ( $\Delta p/p$  of the order of 1%), over a large momentum range ( $p$  from 0.1 GeV/c to 10-12 GeV/c) [15]. The tracking algorithm has also been proven to be sufficiently fast to deal with the high multiplicity environment in heavy ion reactions and the very high collision rates foreseen [17].

The MVD detector [18] will serve for the identification of open charm hadrons through the reconstruction of their displaced decay vertex. This is crucial to reject the tremendous background which originates dominantly from the collision vertex. The setup consists of up to 4 stations of thin and highly granular CMOS silicon pixel sensors (see Figure 6). The stations are both stabilized and cooled by a low mass (diamond) support structure and placed inside a vacuum vessel to limit the effect of multiple scattering of produced particles with air molecules (see Figure 7). The vacuum chamber is mounted to the front side of the STS, while the MVD detector itself is mounted on a flange and can be removed without opening the STS volume. This is an important feature to allow the replacement of MVD sensors (about once per year) to deal with the very high collision rates foreseen by CBM and the expectedly large radiation doses received by these sensors.

Detector simulations, including a realistic material budget and CMOS typical performance, demonstrate that the decay vertex of open charm hadrons in typical environments in CBM at FAIR (e.g. collision system, energy and centrality) can be reconstructed with a resolution below 100  $\mu\text{m}$  [10]. It is, for instance, of 52  $\mu\text{m}$ , 56  $\mu\text{m}$  and 69  $\mu\text{m}$  for  $D^0$  mesons ( $c\tau \sim 123 \mu\text{m}$ ),  $D^{+/-}$  mesons ( $c\tau \sim 312 \mu\text{m}$ ) and  $\Lambda_c^+$  baryons ( $c\tau \sim 60 \mu\text{m}$ ), respectively. An example of the expected resolution for the  $D^+ \rightarrow \pi^+ \pi^+ K^-$  signal in central Au(25 GeV/nucleon)+Au collisions is shown in Figure 10.

The TOF detector, in combination with the STS providing particle momenta, aims at identifying hadrons. It consists of timing resistive plate chambers, which feature a time resolution of about 80 ps [19]. As shown in Figure 11, this high resolution allows separating protons and kaons up to about  $p=6$  GeV/c [16] (at momenta above 6 GeV/c, the rate of particles is relatively low in nucleus-nucleus collisions at FAIR energies). Pions and kaons can also be distinguished up to about  $p=3$  GeV/c.

As for the identification of electrons, a combination of RICH and TRD detectors will be used. Note that the latter detector also serves for global track reconstruction by connecting the tracks reconstructed in the STS with the TOF and ECAL detectors.

The RICH detector will be located directly after the STS. It consists of a  $\text{CO}_2$  gas radiator, float glass mirrors, and Multi-Anode Photo-Multiplier Tube (MAPMT) detectors located in the focal plane

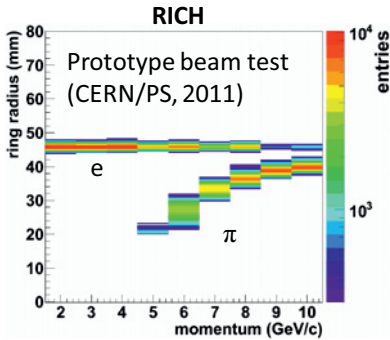


**Figure 12.** Ring radius measured for electrons and pions in the RICH detector prototype as a function of momentum during the 2011 beam test at the CERN-PS [20].

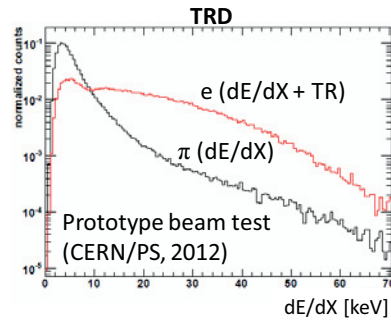


**Figure 13.** Energy deposition per unit path measured for electrons (red histogram) and pions (black histogram) at  $p=3$  GeV/c in the TRD detector prototype during the 2012 beam test at the CERN-PS [21].

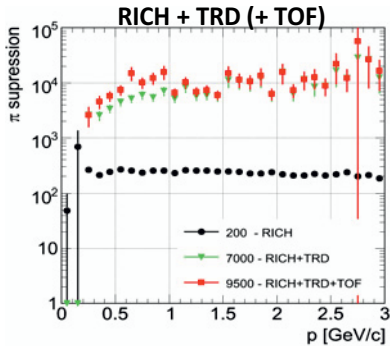


**Figure 14.** Suppression factor for pions mis-identified as electrons as a function of momentum, obtained with combined RICH, TRD (and TOF) information in central Au(25 GeV/nucleon)+Au collisions.

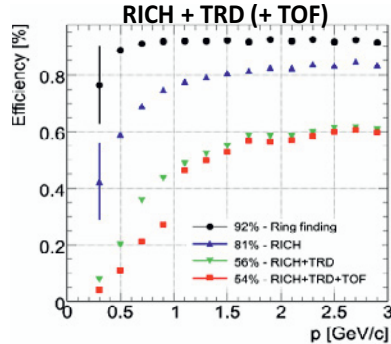


**Figure 15.** Electron reconstruction efficiency as a function of momentum, obtained (together with the pion suppression factor shown on the left side) with combined RICH, TRD (and TOF) information in central Au(25 GeV/nucleon)+Au collisions.

of the mirrors (and shielded from direct tracks by the magnet yokes). The Cherenkov light produced by charged particles in the radiator gas is reflected to the MAPMT detectors producing rings of collected photons. As can be seen in Figure 12, electrons and pions can be well separated up to  $p=10$  GeV/c [20].

The TRD detector is composed of three stations constituted of four layers each. Each layer comprises a mixed (80% Xe + 20% CO<sub>2</sub>) gas radiator where the transition radiation is produced and a Multi-Wire Proportional Chamber detector measuring the energy deposited by charged particles and the transition radiation. The additional transition radiation from electrons (see Figure 13) allows, based on a statistical analysis, discriminating them from pions [21].

As shown in Figures 14 and 15, detailed simulation studies demonstrate that the combined RICH and TRD detectors can be used to suppress pions mis-identified as electrons by about a factor of  $10^4$ , while keeping the electron reconstruction efficiency of the order of 50-60 % at momenta above 1 GeV.

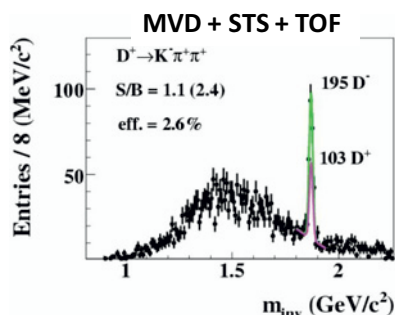


**Figure 16.** Invariant mass of  $\pi^+ \pi^+ K^-$  triplets surviving the selection procedure (including  $D^+$  signals and background triplets) in central Au(25 GeV/nucleon)+Au collisions.

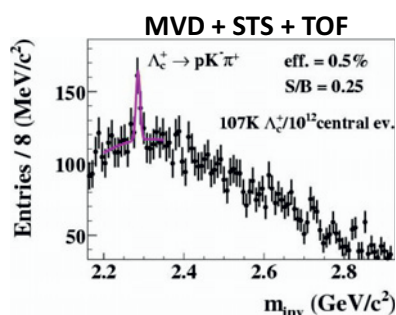


**Figure 17.** Invariant mass of proton  $K^- \pi^+$  triplets surviving the selection procedure (including  $\Lambda_c^+$  signals and background triplets) in central Au(25 GeV/nucleon)+Au collisions [10].

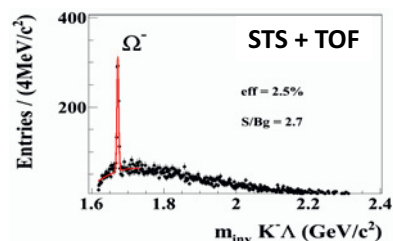


**Figure 18.** Invariant mass of  $K^- \Lambda$  pairs surviving the selection procedure (including  $\Omega^-$  signals and background pairs) in central Au(25 GeV/nucleon)+Au collisions.

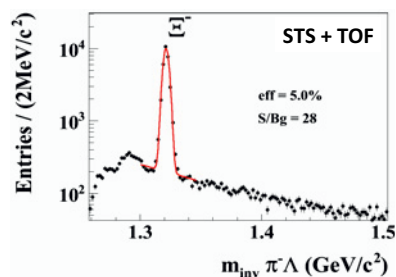


**Figure 19.** Invariant mass of  $\pi^- \Lambda$  pairs surviving the selection procedure (including  $\Xi^-$  signals and background pairs) in central Au(25 GeV/nucleon)+Au collisions.

At lower momenta, the TOF information can also be used to further improve the suppression of pions mis-identified as electrons.

The extremely high particle flux expected through the detector (up to several  $10^9$  particles per second) calls for very high speed, free streaming data read-out, which is a unique feature compared with previous heavy ion experiments. The data will be transported to a large and high performance processor farm with about 60000 computing cores, where event reconstruction (tracking, vertexing, etc) and ultra fast on-line event selection will be performed in real time [22, 23]. This will allow selecting events which contain signal candidates (e.g. open charm displaced decay vertex,  $J/\psi$  decay muons [24]), making it possible to operate at the foreseen collision rates while keeping the event archiving rate at an acceptable level, of the order of 25 kHz.

### 3.2 Physics performance

Detailed detector simulations have been carried out, including realistic background generation and detector description. They demonstrate the detector performance for reconstructing the various probes foreseen by the experiment, including rare probes. Examples of the expected performance are shown in Figures 16 - 21 for central Au(25 GeV/nucleon)+Au collisions.

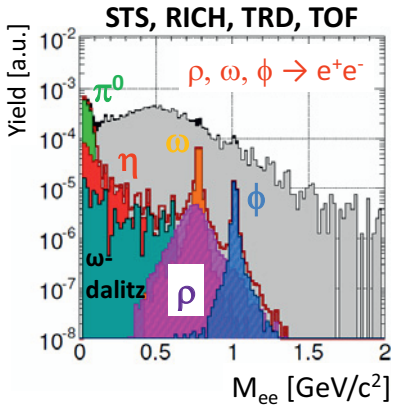


**Figure 20.** Invariant mass of  $e^+ e^-$  pairs surviving the selection procedure (including light vector meson signals - magenta, orange and blue histograms - and background pairs) in central Au(25 GeV/nucleon)+Au collisions [25].

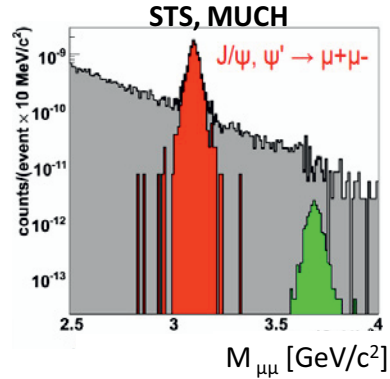


**Figure 21.** Invariant mass of  $\mu^+ \mu^-$  pairs surviving the selection procedure (including  $J/\psi$  meson signals - red histogram,  $\psi'$  meson signals - green histogram - and background pairs) in central Au(25 GeV/nucleon)+Au collisions.

As can be seen in Figure 16, the  $D^+ \rightarrow \pi^+ \pi^+ K^-$  signal can be extracted from the combinatorial background with high signal-to-background ratio and good reconstruction efficiency, thanks to the high vertexing precision provided by the MVD. As for  $\Lambda_c^+$  baryons, their measurement is a particularly challenging task (see Figure 17) because of their extremely short lifetime [10]. It is important to stress that this measurement will benefit from the rapid improvements of the rate capability of CMOS silicon pixel sensors [26, 27].

Multi-strange hadrons can also be extracted from the background with high signal-to-background ratio and good reconstruction efficiency (see Figures 18 and 19). Note that the MVD is not needed for this task because of the longer lifetime of these particles with respect to that of open charm hadrons.

Light vector mesons in their di-electron decay channel (see Figure 20) can be measured with satisfactory signal-to-background ratio (about one order of magnitude higher with respect to CERES data [28]) and good reconstruction efficiency [25]. The contamination of the electron sample by mis-identified hadrons is strongly reduced when the combined RICH, TRD and TOF information is exploited. The remaining background is dominated by electrons from  $\gamma$ -conversion in the target and  $\pi^0$  Dalitz decays. Let us remind that, alternatively to the di-electron channel, light vector mesons can be detected via their decay into muon pairs. It is achieved by selecting and identifying tracks which pass the five first absorber layers of the MUCH detector (which represent about 8 times the nuclear interaction length) as potential decay muons of light vector mesons. A drawback of the 'muon' setup is that only the mass region above the two-muon threshold can be accessed. In this region, this alternative method provides a crosscheck of the di-electron measurement.

In the 'muon' configuration,  $J/\psi$  mesons can be measured with high signal-to-background ratio (see Figure 21) and good reconstruction efficiency. It is achieved by selecting and identifying tracks which pass the full absorber material (which represents about 14 times the nuclear interaction length) as potential decay muons of  $J/\psi$  mesons. This method allows reducing drastically hadrons mis-identified as  $J/\psi$  decay muons, the remaining background being dominated by muons from weak decays of pions and kaons before the MUCH absorbers. It is important to stress that another advantage of the di-muon channel measurement is that, the background being low, a trigger on  $J/\psi$  decay muon

candidates is feasible which allows operating at the maximal collision rate foreseen by the experiment (10 MHz) [24].

## 4 Status of preparation

All detector components are now at the stage of prototyping and are being tested in beam, and technical design reports are either submitted (see e.g. [14]) or in the process of submission. The construction phase of the FAIR accelerator is planned to end in 2017, when the experiment apparatus will be installed in the CBM cave. First measurements with nuclear collisions will start in 2019 at the SIS100 synchrotron, which will provide, for the first time, charm data in p+p and p+A collisions at about 30 GeV beam energy and below, and will allow the investigation of very interesting strangeness physics in A+A collisions up to 10 GeV/nucleon.

## References

- [1] Z. Fodor and S. D. Katz, *JHEP* **03**, 014 (2002)
- [2] P. de Forcrand *et al.*, *PoSLAT2007* **178** (2007)
- [3] C. Alt *et al.*, *Phys. Rev. C* **77**, 024903 (2008)
- [4] B. I. Abelev *et al.*, *Phys. Rev. C* **81**, 024911 (2010)
- [5] M. Lutz *et al.*, *Nucl. Phys. A* **542**, 521 (1992)
- [6] M. Stephanov, *Journal of Physics: Conference Series* **27**, 144-153 (2005)
- [7] M. Stephanov, *Prog. Theor. Phys. Suppl.* **153**, 139-156 (2004)
- [8] I. C. Arsene *et al.*, *Phys. Rev. C* **75**, 034902 (2007)
- [9] P. Braun-Munzinger *et al.*, arXiv:nucl-th/0304013v1 (2003)
- [10] B. Friman *et al.*, *The CBM physics book*, *Lect. Notes Phys.* **814** (Springer, Berlin, 2011), 1-980
- [11] A. Andronic *et al.*, *Phys. Lett. B* **659**, 149-155 (2008)
- [12] P. Senger *et al.*, *CBM Progress Report 2012*, 1-2 (2013)
- [13] T. Tischler, PhD thesis, to be published
- [14] J. Heuser *et al.*, *Technical design report for the CBM Silicon Tracking System (STS)*, GSI Report 2013-4 (2013)
- [15] V. Friese and A. Kotynia, *CBM Progress Report 2012*, 25 (2013)
- [16] I. Vassiliev *et al.*, *CBM Progress Report 2012*, 101 (2013)
- [17] V. Akishina *et al.*, *CBM Progress Report 2012*, 92-93 (2013)
- [18] S. Seddiki, PhD thesis, Strasbourg and Frankfurt (2012)
- [19] A. Laso Garcia *et al.*, *CBM Progress Report 2012*, 73 (2013)
- [20] J. Kopfer *et al.*, *CBM Progress Report 2012*, 27-28 (2013)
- [21] C. Bergmann *et al.*, *CBM Progress Report 2012*, 57 (2013)
- [22] J. de Cuveland *et al.*, *CBM Progress Report 2012*, 89 (2013)
- [23] V. Akishina *et al.*, *CBM Progress Report 2012*, 92 (2013)
- [24] V. Singhal *et al.*, *CBM Progress Report 2012*, 97 (2013)
- [25] E. Lebedeva and C. Höhne, *CBM Progress Report 2012*, 106 (2013)
- [26] M. Winter *et al.*, *CBM Progress Report 2011*, 6 (2012)
- [27] D. Döring *et al.*, *CBM Progress Report 2012*, 7 (2013)
- [28] G. Agakichiev *et al.*, *Phys. Lett. B* **422**, 405-412 (1998)